Supporting information

Grain Engineering for Improved Charge Carrier Transport in Two-Dimensional Lead-Free Perovskite Field-Effect Transistors

Shuanglong Wang[1], Sabine Frisch[2], Heng Zhang[1], Okan Yildiz[1], Mukunda Mandal[1], Naz Ugur[1], Beomjin Jeong[1], Charusheela Ramanan[1], Denis Andrienko[1], Hai Wang[1], Mischa Bonn[1], Paul W. M. Blom[1], Milan Kivala[2], Wojciech Pisula,[1,3,*] and Tomasz Marszalek[1,3,*]

1 Max Planck Institute for Polymer Research, Ackermannweg 10, 55128 Mainz, Germany

2 Organisch-Chemisches Institut, Centre for Advanced Materials, Ruprecht-Karls-Universität Heidelberg, 69120 Heidelberg, Germany

3 Department of Molecular Physics, Faculty of Chemistry, Lodz University of Technology, Zeromskiego 116, 90-924 Lodz, Poland

*To whom correspondence should be addressed.

Email: pisula@mpip-mainz.mpg.de, marszalek@mpip-mainz.mpg.de

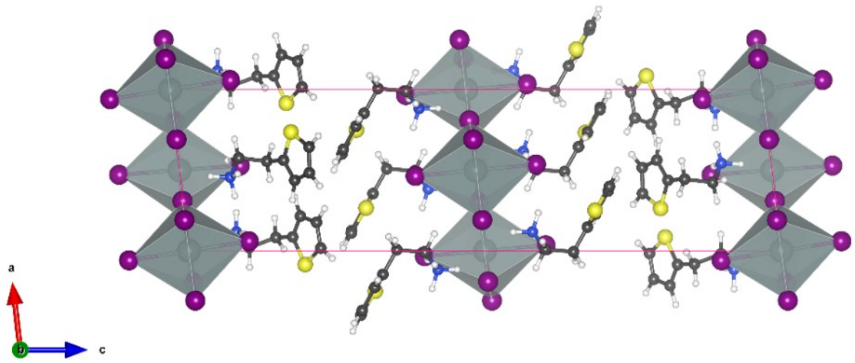

Optimized lattice parameters	
a (Å)	8.5681
b (Å)	8.5775
c (Å)	31.5384
α (°)	96.5431
β (°)	96.5979
γ (°)	90.1130

Figure S1. PBE-D3(0)-optimized structure and lattice parameters for $(TEA)_2SnI_4$.

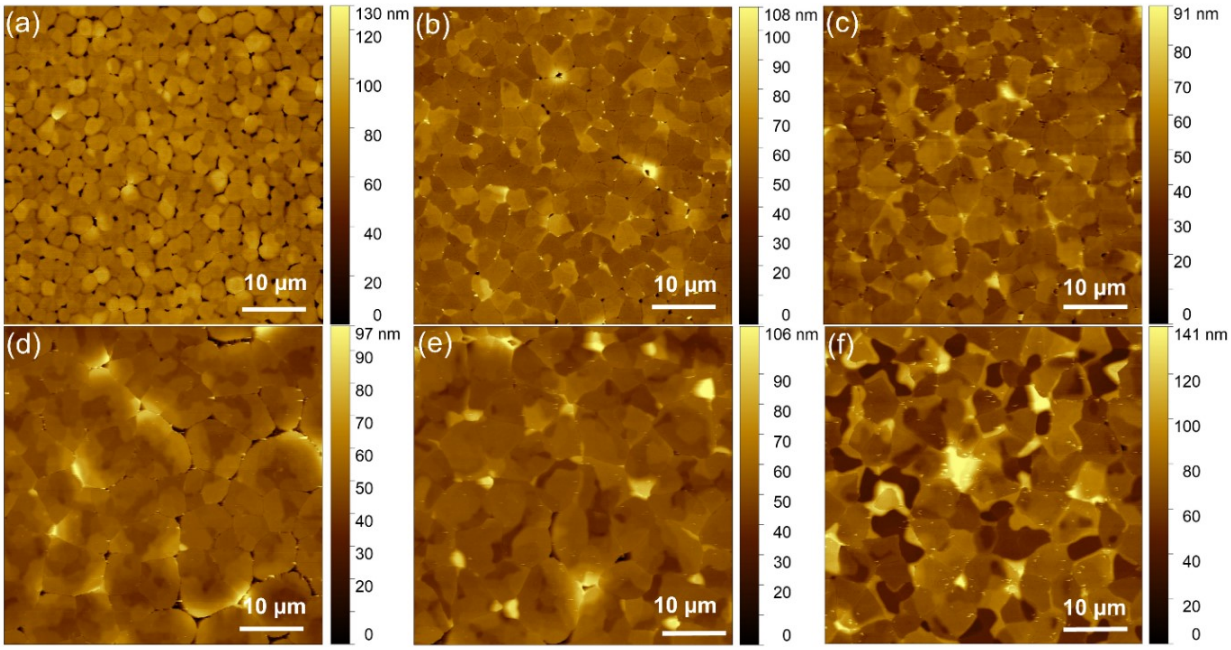

Figure S2. Large scan size of AFM images of $(TEA)_2SnI_4$ films cast at the temperature of (a) RT, (b) 80 °C, (c) 100 °C, (d) 120 °C, (e) 140 °C, and (f) 160 °C.

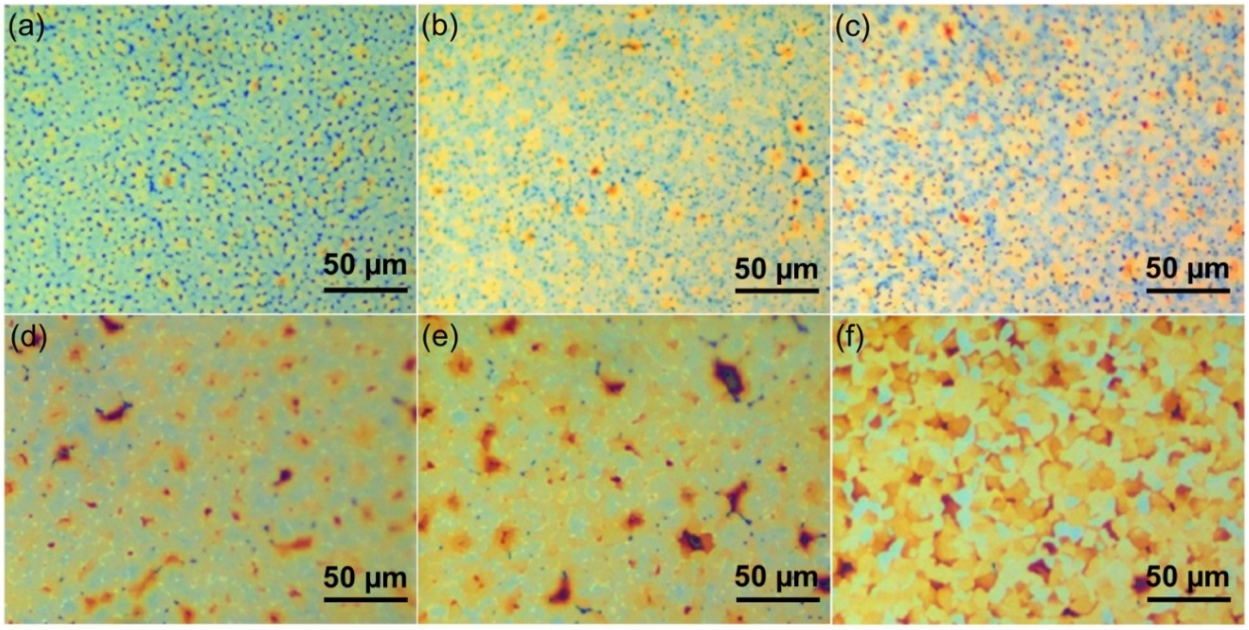

Figure S3. Optical microscope images for 2D $(TEA)_2SnI_4$ perovskite thin films cast at substrate temperature of (a) RT, (b) 80 °C, (c) 100 °C, (d) 120 °C, (e) 140 °C and (f) 160 °C.

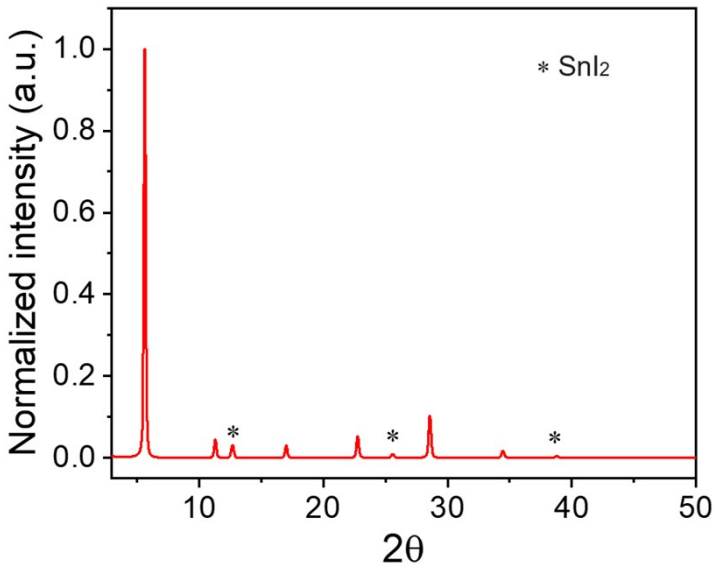

Figure S4. XRD pattern of the $(TEA)_2SnI_4$ thin film prepared with hot-casting method at 140 °C.

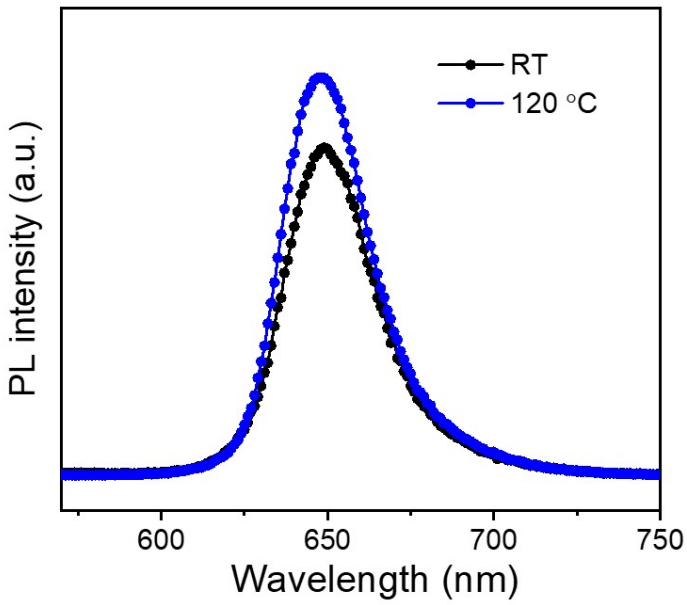

Figure S5. PL spectra of the 2D $(TEA)_2SnI_4$ perovskite thin films cast at RT and 120 °C.

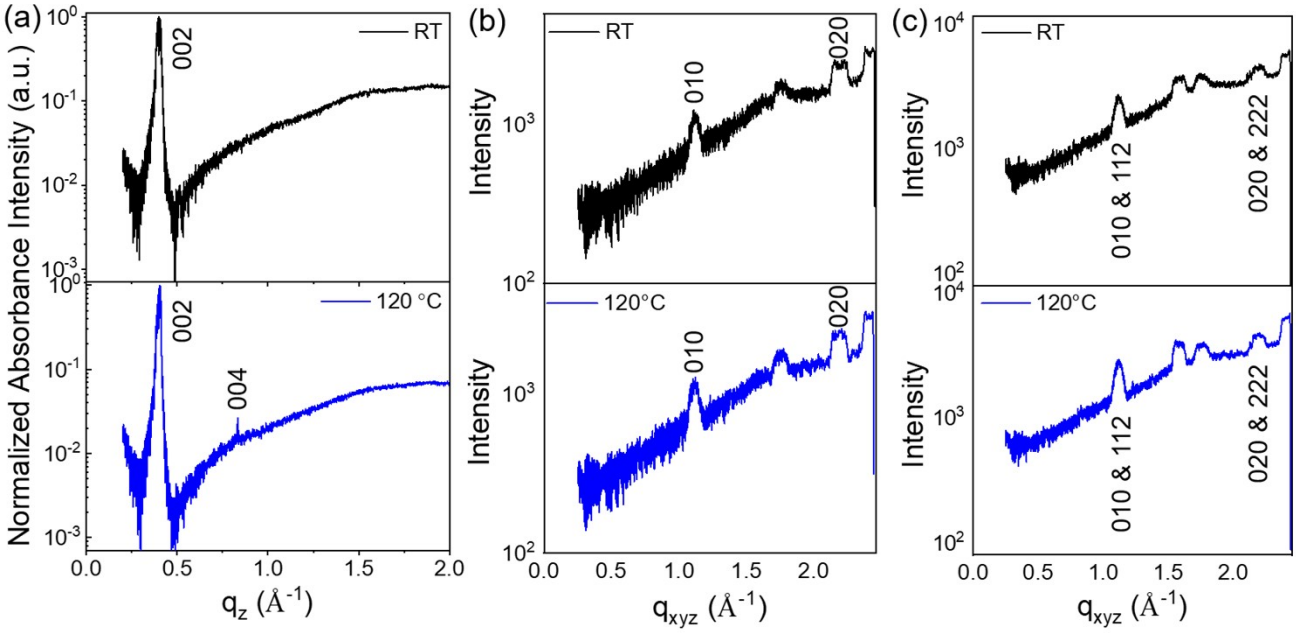

Figure S6. Profiles of GIWAXS patterns for (a) out-of-plane, (b) α_{5° and (c) α_{10° of $(TEA)_2SnI_4$ films cast at RT and 120 °C.

Table S1. The d-spacings determined from GIWAXS pattern.

Bonding types	Distance (Å)	hkl
Interlayer distance	15.7	002
I-Sn-I	5.8	010
I-Sn	2.9	020
I-I	4.1	120

Frequency-resolved THz photoconductivity and its fitting to Drude-Smith model

To gain more insights into the charge carrier transport, the frequency-resolved complex photoconductivity spectrum was recorded (at the pump-probe delay time of 3.2 ps as indicated in the dynamics) and is presented in Figure S6. For both deposition conditions at RT and 120 °C, a unique combination of the significant real and nearly zero imaginary contributions to the photoconductivity are observed, indicating a free carrier-dominant charge transport behavior. [1] To quantitatively compare the charge transport in films from both deposition temperatures, the spectra were fitted by Drude-Smith (DS) model, which describes the free carrier transport in a medium with spatial confinement. The model reads: [1,2]

$$\sigma(\omega) = \frac{\omega_p^2 \varepsilon_0 \tau}{1 - i\omega\tau}\left(1 + \frac{c}{1 - i\omega\tau}\right) \quad (3)$$

where ω_p is the plasma frequency ($\omega_p = \sqrt{\frac{n}{\varepsilon_0 \cdot m^*}}e$, m^* is the effective mass), τ is the charge scattering time, ε_0 is the vacuum permittivity, ω is the angular frequency. Different from the classical Drude model, the DS model takes into account the

anisotropic backscattering effect due to e.g., presence of the grain boundaries by a parameter c ranging between 0 and -1. For $c = 0$, the DS model describes simply the Drude conductivity in which the free carriers transport with isotropic momentum scattering. For $c =$ -1, free carriers are assumed to experience strongly spatial confinement with 100% backscattering. From the fitting, we can infer the plasma frequency ω_p (related to charge carrier density *n*), *c* parameter, and charge scattering time τ. Both ω_p and c parameters are found to be very similar, confirming our assumption of the same photon-to-carrier conversion efficiency and indicating the identical back scattering effect in both samples. On the other hand, the change in the scattering time dominates the charge transport, with $\tau =$ 66 ± 4 fs and 50 ± 5 fs for 120 °C and RT cast films, respectively. Based on the inferred transport parameter, we estimate the charge carrier mobility in the *dc* limit, following $\mu = \frac{e \cdot \tau}{m^*} \cdot (1 + c)$. This indicates a 28% mobility enhancement from 207 ± 21 $cm^2V^{-1}s^{-1}$ for RT deposited samples to 265 ± 16 $cm^2V^{-1}s^{-1}$ for the 120 °C hot cast film. Combining the similar photoconductivity enhancement observed (in the OPTP data), our analysis on the frequency-resolved conductivity indicates the dominant role of charge scattering time on determining the charge carrier mobility.

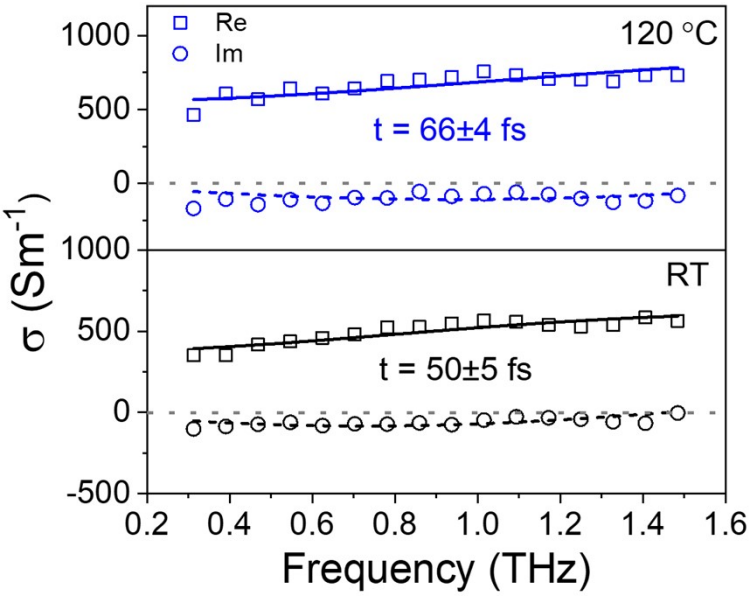

Figure S7. Frequency-resolved photoconductivity spectra and corresponding Drude-Smith fittings for $(TEA)_2SnI_4$ films cast at RT and 120 °C.

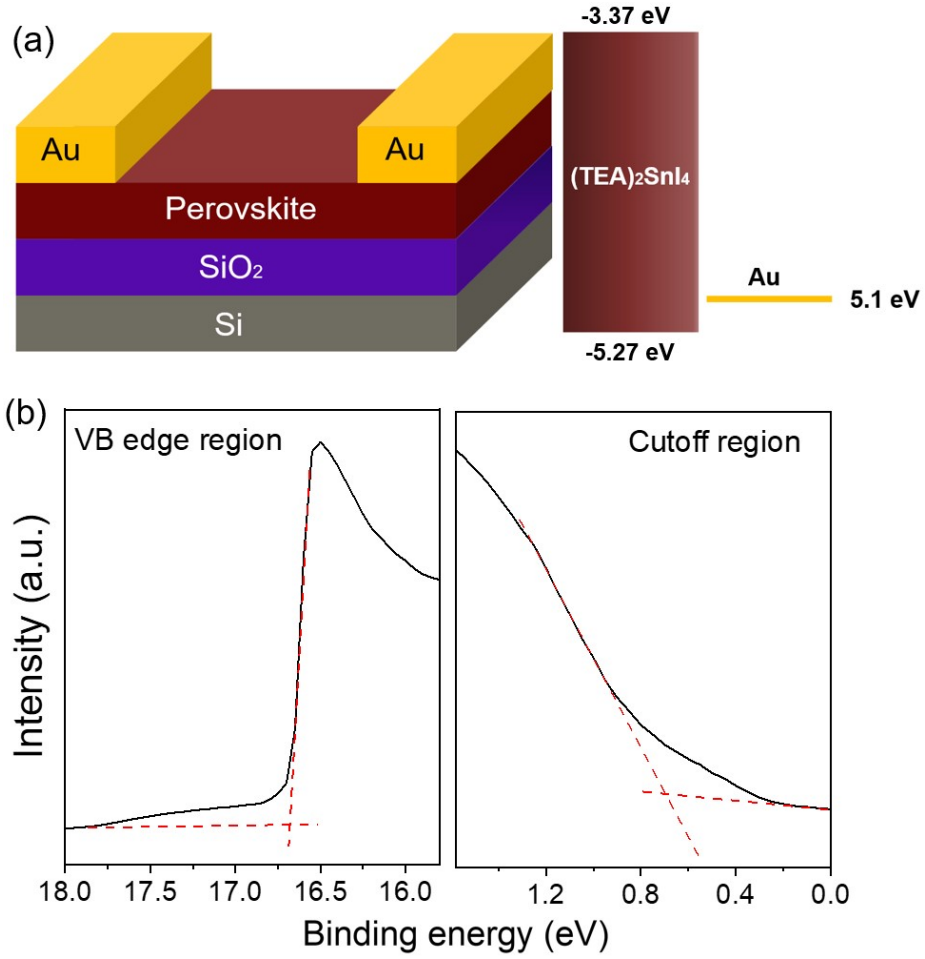

Figure S8. (a) Schematic of the bottom-gate top-contact $(TEA)_2SnI_4$ FET device structure and the energy level of $(TEA)_2SnI_4$ semiconductor film and Au electrode. (b) Ultraviolet photoelectron spectroscopy (UPS) of $(TEA)_2SnI_4$ perovskite thin film.

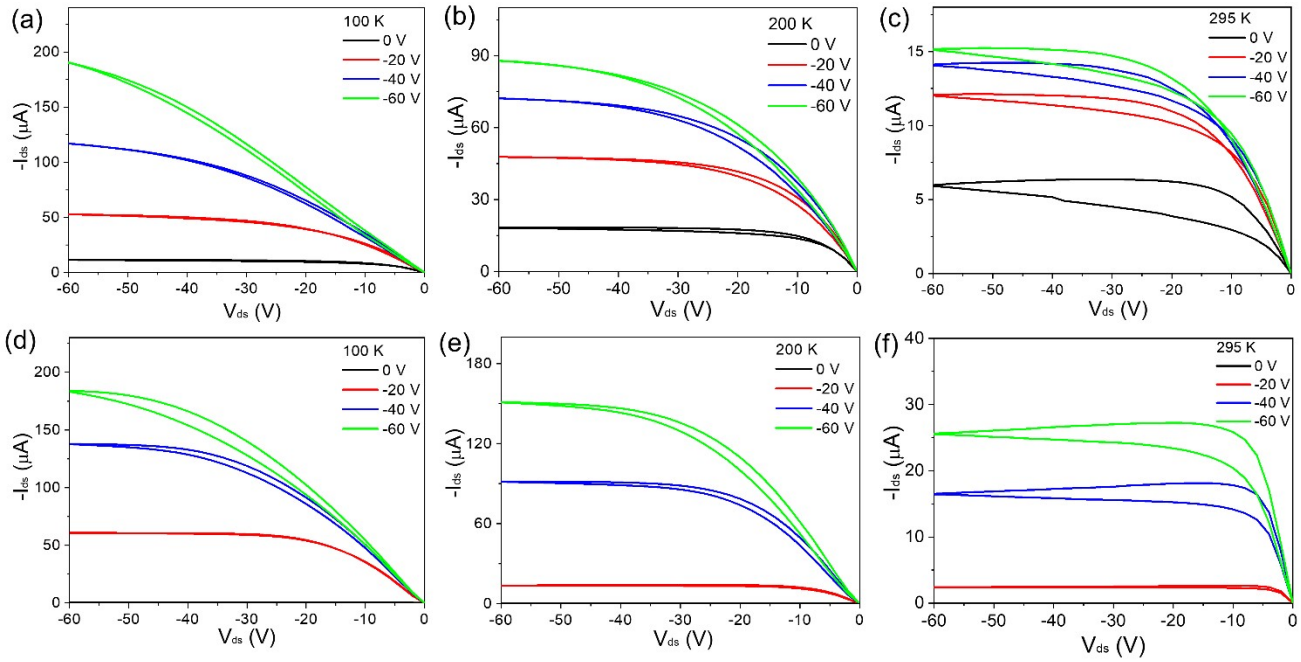

Figure S9. Output characteristics of bottom-gate top-contact FET devices at (a) 100 K, (b) 200 K and (c) 295 K prepared at RT and (d-f) corresponding hot-casting method at 120 °C.

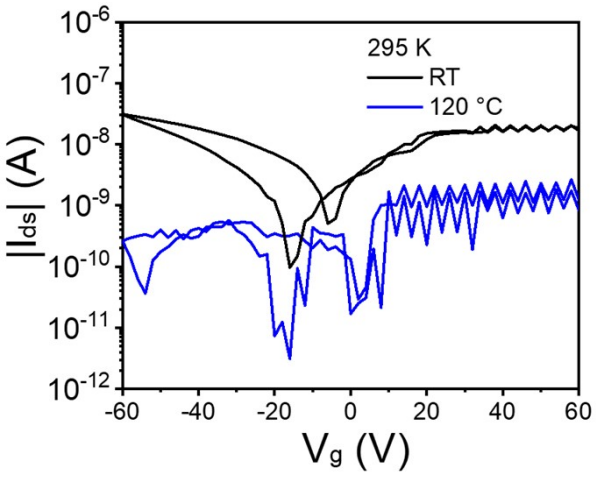

Figure S10. Raw data of gate leakage currents for RT and hot-casting prepared FET devices at 295 K.

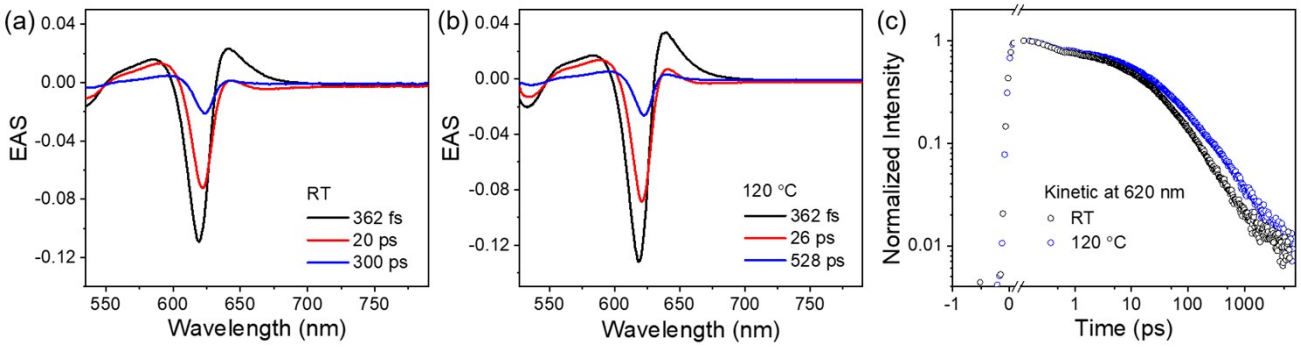

Figure S11. Time resolved transient absorption spectra of the 2D $(TEA)_2SnI_4$ perovskite layers prepared at (a) room temperature and (b) 120 °C by hot-casting. Delay times are indicated in the plots. (c) Kinetic traces at probe wavelength of 620 nm for the two perovskite films.

The excited state dynamics of the samples was measured using transient absorption spectroscopy. The samples were photoexcited at 529 nm. Global analysis of the data using a 3-compartment model yields the evolution associated difference spectra (EADS) in Figure S11a and b. The transient spectra for the two samples are very similar. Negative peaks <550 nm and at 625 nm correspond to the ground-state bleach (GSB) and there is an overlapping excited state absorption between 550-700 nm. The spectral evolution and the three components fit correlate with literature report of other 2D Sn-based perovskites [3]. While the spectral evolution of room temperature and hot-cast films are similar, the excited state decay dynamics differ. Hot-cast perovskite sample

exhibits a longer excited state lifetime than reference sample, evidenced by the comparison of the transient kinetics at 620 nm (Figure S11c) and the slower decay rates from the global fit. The measured photoluminescence quantum yield (PLQY) values for the two perovskite films prepared at room temperature and 120 °C are 0.1% and 0.2%, respectively. The slower excited state decay and higher PLQY value of hot-cast film is consistent with a relative reduction in non-radiative decay from defect sites.

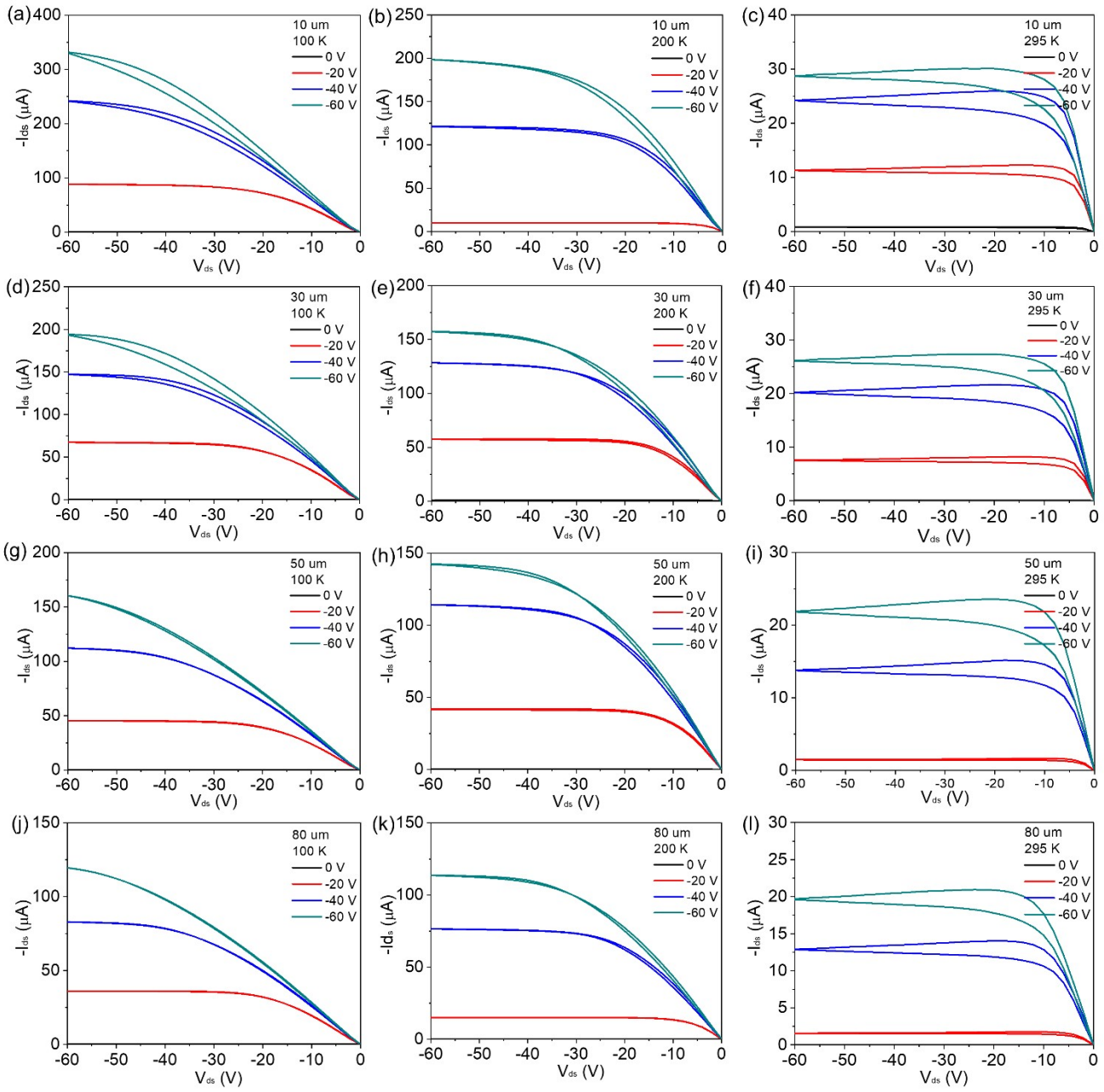

Figure S12. Output characteristics of bottom-gate top-contact FET devices with different channel length at (a) 100 K, (b) 200 K and (c) 295 K prepared by hot casting method at 120 °C.

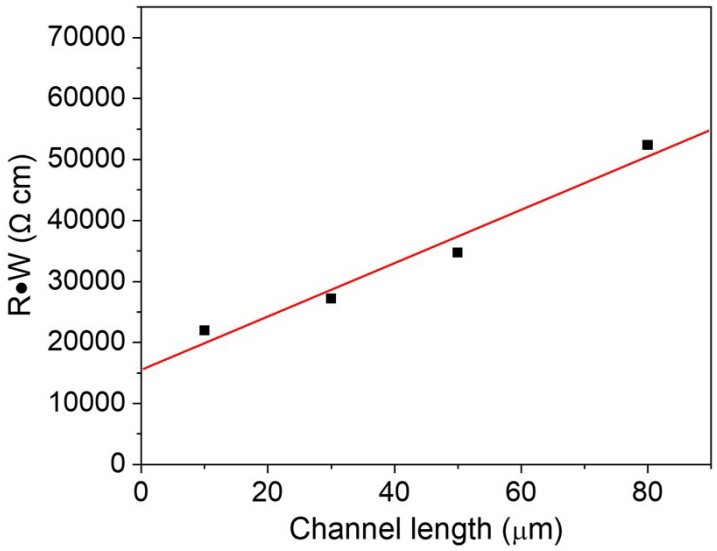

Figure S13. The plot of R·W as a function of channel length for 120 °C hot-cast perovskite FET at 295 K. The contact resistance is determined from the y-axis intercept

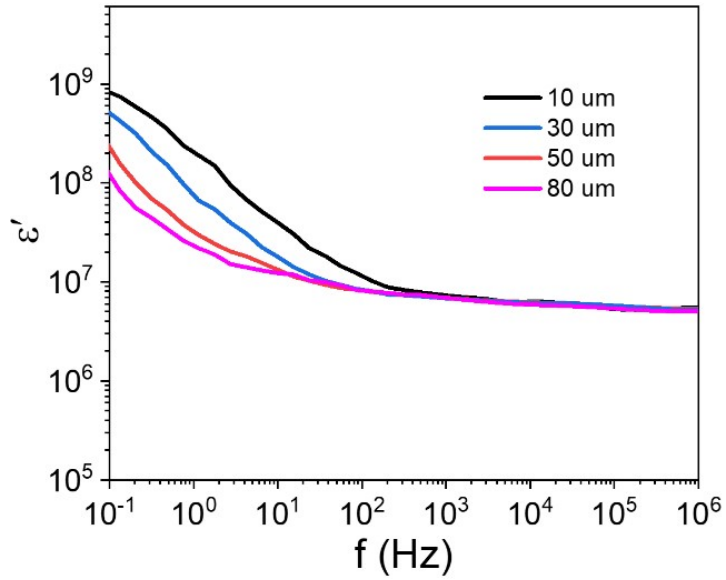

Figure S14. The real part of dielectric constant for perovskite films as a function of frequency measured in the top contact geometry for different channel lengths.

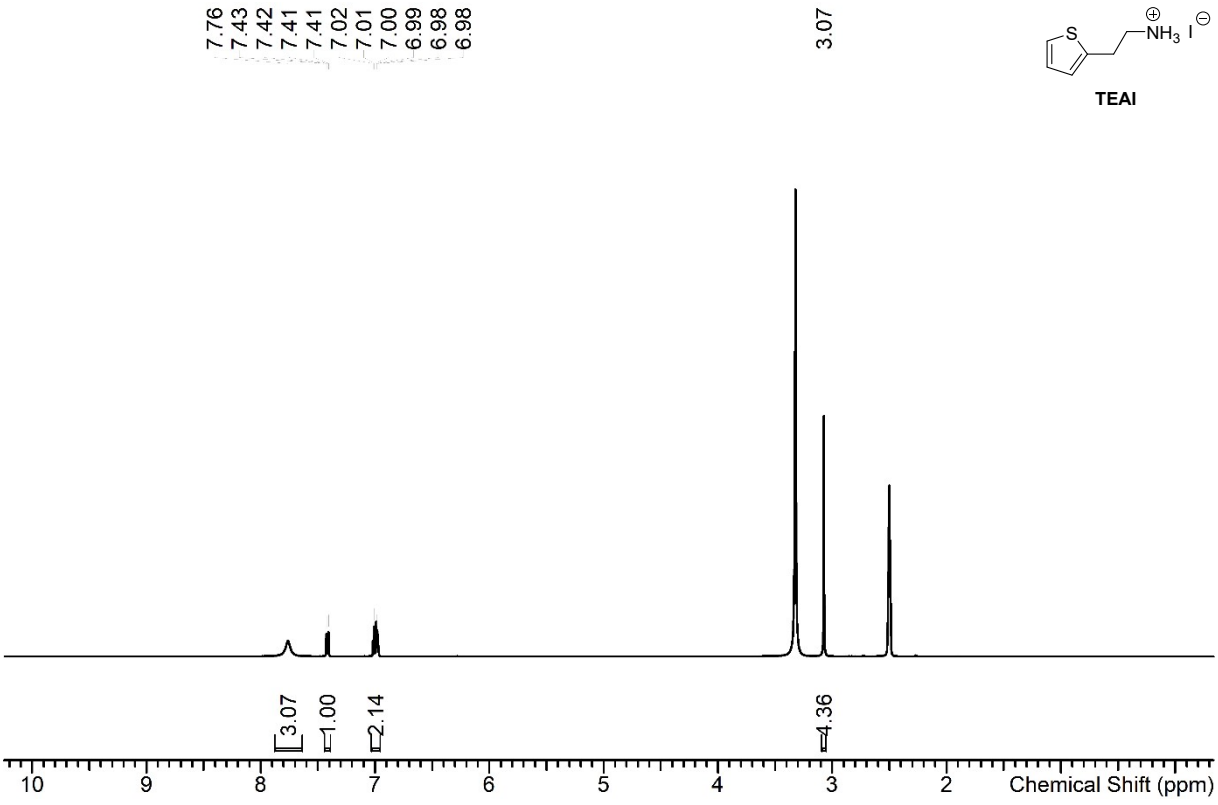

Figure S15. ^{1}H NMR (300 MHz, $(CD_3)_2SO$) spectrum of TEAI. *H_2O.

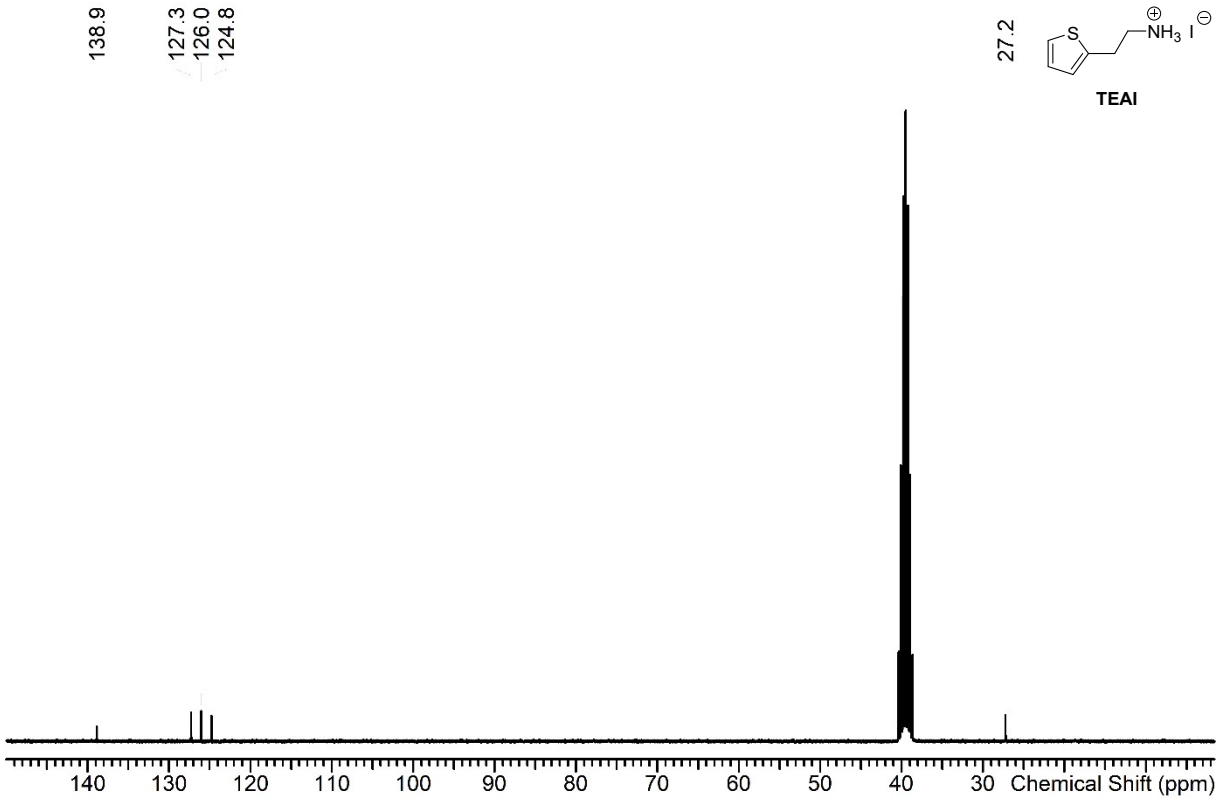

Figure S16. ^{13}C NMR spectrum (76 MHz, $(CD_3)_2SO$) of TEAI.

Supplementary References:

1. Ulbricht, R. et al. Carrier dynamics in semiconductors studied with time-resolved terahertz spectroscopy. Reviews of Modern Physics, **83**, 543 (2011).
2. Smith, N. V. Drude theory and the optical properties of liquid mercury. Physics Letters A, **26**, 126-127 (1968).
3. Zhang, T, R. et al. Regulation of the luminescence mechanism of two-dimensional tin halide perovskites. Nature communications, **13**, 1-11 (2022).